JOURNAL OF COASTAL AND RIVERINE FLOOD RISK

Vol. 3, 2024, 15

Probabilistic Tsunami Hazard Assessment from Manila Trench to Shantou City in China

Tingyu Zhang[1], Miguel Esteban [2], Takahito Mikami[3], Tomoya Shibayama[4]

[1]zhangtingyu29172@akane.waseda.jp, Waseda University, Tokyo, Japan
[2]esteban.fagan@gmail.com, Waseda University, Tokyo, Japan
[3]takahito8765@gmail.com, Waseda University, Tokyo, Japan
[4]shibayama@waseda.jp, Waseda University / Chuo University, Tokyo, Japan

Research article. Submitted: 02 March 2025, **Reviewed:** 06 November 2024, **Accepted:** 01 December 2024, **Published:** 16 December 2024

DOI: https://doi.org/10.59490/jcrfr.2024.0015

Cite as: "Zhang, T., Miguel, E., Mikami, T., & Shibayama, T. Probabilistic Tsunami Hazard Assessment from Manila Trench to Shantou City in China. *Journal of Coastal and Riverine Flood Risk* . https://doi.org/10.59490/jcrfr.2024.0015".

Abstract

Despite the well-known tsunami hazards originating from the Manila Trench, a detailed assessment of present and future risks to the South coastline of China has not been made. Thus, the present paper analyzes the tsunami hazard at the southern coastline of China, and more specifically at the city of Shantou. A Monte Carlo-type probabilistic tsunami hazard assessment (PTHA) with 5000 simulation runs was conducted using the tsunami propagation model COMCOT. A wide range of earthquake magnitudes were stochastically simulated in these zones, ranging from 7.0 to 9.0 in magnitude, and the peak nearshore tsunami amplitude (PNTA), for return periods of 100, 1,000 and 10,000 years, was determined by propagation simulations to be 0.15 m, 0.65 m and 1.75 m, respectively. Inundation simulations for the case study area, which considered various scenarios of sea level rise between the present day and the year 2100, were also conducted. The results indicate the severe influence that sea level rise could have on tsunami risks, which can provide valuable information for disaster risk managers and planners on how to develop adaptation pathways not only for this city but also for other points along the southeast coastline of China.

Keywords

Tsunami propagation simulations, PTHA, Manila Trench, Monte Carlo type, COMCOT, Tsunami inundation simulations, Sea level rise.

1 Introduction

Manila Trench lies to the west side of Luzon Island in the Philippines, within the east portion of the South China Sea, and has been assessed as a high-risk tsunami source by USGS (Kirby et al. 2006). The most recent historical record of a tsunami hazard caused by a movement in the Manila Trench was generated to the southwest of Taiwan on Dec. 26, 2006, when two offshore earthquakes with Mw 7.0 generated a wave with a height of 0.05 m above the normal tide level (NOAA, Yi et al., 2007). Most of the sections of Manila Trench have accumulated strain over the last 440 years, and thus this tsunamigenic zone represents a significant potential risk to the coastal areas around it (Wu and Huang, 2009).

This paper aims to analyze the tsunami hazard around the south coasts of China, taking Shantou city as its target area. Shantou sits to the east of Guangdong Province, facing the South China Sea to the southeast, and is a significant trading port and commodity distribution center, as shown in Fig. 1. The last recorded tsunami in Shantou took place on Feb 13th, 1918, when after an earthquake with M. 7.5 the sea surged and the rocky hills along the coast collapsed (NOAA, Gu et al. 1989). Previous research by Hou et al. (2014) indicated that a tsunami from Manila Trench could result in an inundation of 17 km^2 in Shantou, affecting most companies, schools and hospitals in the east of the city. According to Yingchun et al. (2007), the probability for a tsunami with a height of over one meter to take affect Shantou city in the next 100 years is 43.99%, although these authors only performed propagation simulations, and did not consider the detailed propagation over land close to the city. This clearly highlights the tsunami hazard risks along the southeast coastline of China, and the need for further studies in this geographical area.

The tsunami risks to Shantou are further compounded by ongoing sea level rise (SLR). According to the Intergovernmental Panel on Climate Change (IPCC), the global mean sea level (GMSL) rose faster in the 20th century than in any prior century, with a 0.20 m (0.15 to 0.25 m) rise recorded during the period between 1901 and 2018 (Fox-Kemper, et al., 2021). It is virtually certain that GMSL will continue to rise in the course of the 21st century, and even beyond that. With medium confidence, which considers thermal expansion and the mass loss from glaciers and ice sheets (and not taking into consideration ice-sheet-related processes), GMSL is expected to rise between 0.38 m (SSP1-1.9) and 0.77m (SSP5-8.5) by the year 2100. If Earth processes that are less well understood are considered, likely SLR could reach 1.60 m (SSP5-8.5, with low confidence). It is obvious that SLR changes need to be considered when discussing tsunami risk (Shibayama and Esteban., 2023; Hirschfeld et al., 2024; Esteban et al., 2024), especially in areas where the risk is currently generally considered to be low, such as in the case of Shantou.

The present research will thus quantify the tsunami risk for the city of Shantou, considering future SLR. This will be done by conducting a Monte-Carlo-type probabilistic tsunami hazard assessment (PTHA) using the tsunami propagation model COMCOT (Liu et al. 1998) from the most likely source, the Manila Trench. It should be noted at this point that this research will ignore potential submarine landslide sources closer to mainland China (Ren et al., 2023; submarine landslides have the possibility of generating significant tsunamis, see Takabatake et al. 2022, 2020). While other authors (notably Li et al., 2016) have also conducted tsunami propagation simulations, for a true assessment of the risk posed by such events it is necessary to also perform inundation simulations. A hazard curve explaining the relation between return period and tsunami height will thus be obtained, and tsunami inundation simulations will be conducted using Nays2DFlood for 100, 1,000 and 10,000 years return periods waveforms for a variety of SLR scenarios (for more details on the use of Nays2DFlood see for example Hao et al., 2021 or Ali et al., 2017). The inundation maps that will be provided can serve as a reference for current and future coastal construction and city planning for Shantou, and the methodology followed can inform how similar exercises could be conducted for other cities along the southeast coastline of China.

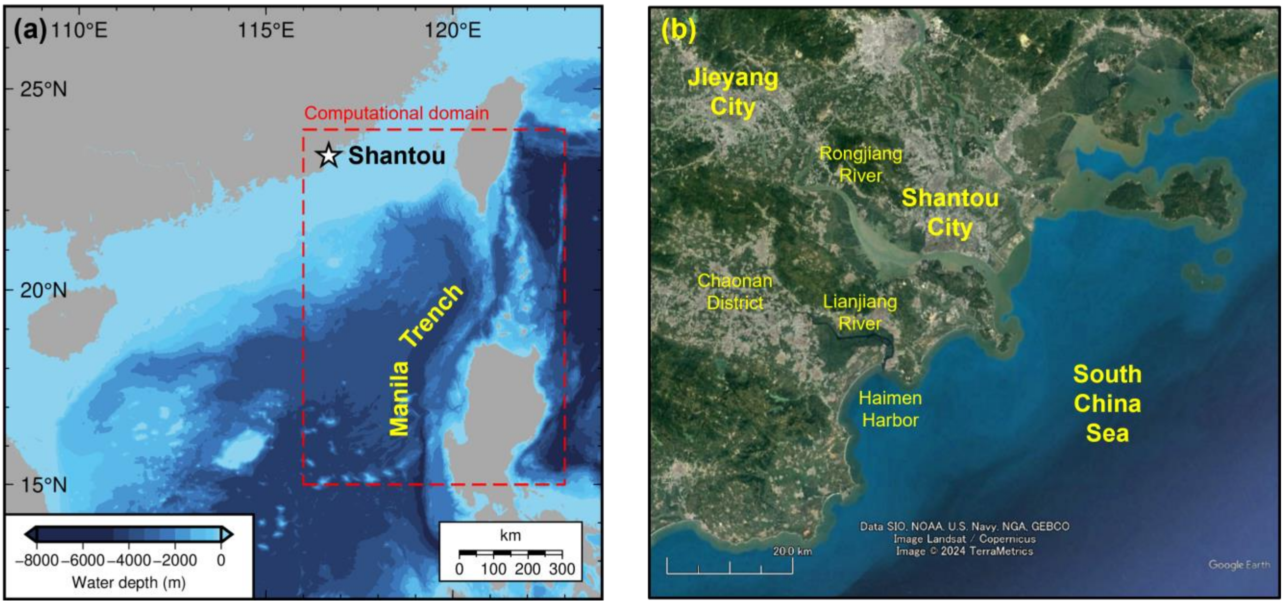

Figure 1: Map of the study area, indicating the location of Manila Trench and Shantou. The extent of the domain used in the propagation simulation is indicated. Data from GEBCO.

2 Methodology

A Monte Carlo type PTHA was utilized in the present study, focusing on the potential tsunami generating region of the northern section of the Manila Trench. The Monte Carlo simulation procedure is shown in Fig. 2. Using the outputs of the PTHA, tsunami inundation simulations were then conducted using Nays2DFlood to map the return periods of the expected inundation extent at Shantou (see Hao et al., 2021 or Ali et al., 2017). Additionally, five patterns of sea level rise (SLR) were considered in the inundation simulation.

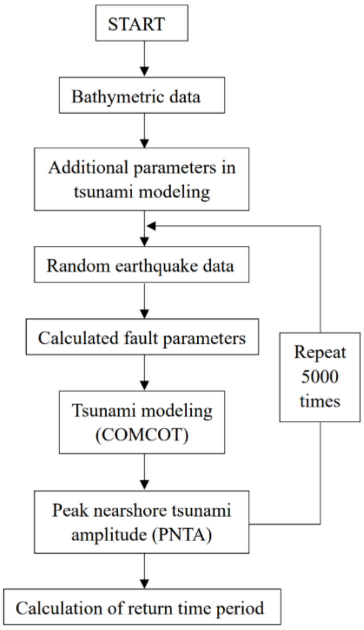

Figure 2: Flow chart of the PTHA.

2.1 Bathymetric data and Manning's roughness coefficient

The bathymetric data used in this study was obtained from GEBCO. GEBCO_2021 Grid is a global terrain model for ocean and land, with the data being provided on a 15-arc second interval (GEBCO Compilation Group 2021). Fig. 1 shows the computational domain used in the tsunami propagation model. A Manning's roughness coefficient of 0.025 was used throughout the simulation propagation domains, similar to that used by other authors (Yingchun et al. 2007, Nagai et al. 2020). The total run time for one simulation was set as 5 hours, with a time step of 0.5 second per step, and the boundary condition was set as open.

2.2 Earthquake data and fault parameters

Each tsunami propagation simulation started by stochastically generating the source of the earthquake. The magnitude and the epicenter of the earthquakes were generated randomly. Jean et al. (2019) showed that there is no relationship between the focal depth of an earthquake and its magnitude (in a study that analyzed the 440 tsunamigenic earthquakes that occurred around the world from 1st January 1970 to 24th August 2018). According to Li et al. (2016) a rupture depth shallower than 50 km can cover 95% of the thrust-type events which are able to generate appreciable tsunami waves. As a result, the focal depth of each earthquake was randomly determined to be between 10 to 50 km.

The length L, width W and the dislocation, which is also called the average slip ΔS of the fault, for each earthquake were calculated according to the earthquake magnitude M_w, using the scaling relations (Papazachos et al. 2004) below:

$$\log_{10} L = 0.55M_w - 2.19 \quad [6.7 \le M_w \le 9.3] \tag{1}$$

$$\log_{10} W = 0.31M_w - 0.63 \quad [6.7 \le M_w \le 9.2] \tag{2}$$

The relationship between the seismic moment M_0, average slip ΔS and the moment magnitude M_w (Peter et al., 2010 and Li et al., 2016) are given by:

$$M_0 = \mu L W \Delta S \tag{3}$$

$$M_w = (\log_{10} M_0 - 9.1)/1.5 \tag{4}$$

where μ represents the rigidity, which is the resistance to moving. According to Peter et al. (2010) and Kanamori (1977), the value of rigidity should be $\mu = 3 - 6 \times 10^{11}$ dyn/cm^2, which is $3 - 6 \times 10^4$ MPa. In the present simulations a value $\mu = 3.035 \times 10^4$ MPa was adopted, following Li et al. (2016).

The strike direction of the fault was measured according to the shape of the Manila Trench, as shown in the research of Li et al. (2016). The dip angle was set to always be 17.9°, under the ideal planar assumption according to Li et al. (2016). The rake angle was also assumed to always be 90° (Wu and Huang, 2009).

2.3 Tsunami propagation simulations

A total of 5000 tsunami propagation simulations were conducted. The earthquake magnitude interval M'_{Wj} can be represented as:

$$M'_{Wj} = \left[M_{Wj} - \frac{\Delta M_{Wj}}{2}, M_{Wj} + \frac{\Delta M_{Wj}}{2}\right] \tag{5}$$

In this study, the authors only considered earthquakes taking place between 15°N and 23°N along Manila Trench (an earlier study by Zhang (2021) indicated that, due to source directionality, only earthquakes originating in this region had the potential to generate tsunamis that could affect the southern coastline of mainland China). As shown in Fig. 3, the northern part of the Manila Trench can be subdivided into two zones, and the numbers of tsunami propagation simulations conducted for different earthquake magnitude intervals in zone A and zone B are shown in Table 1.

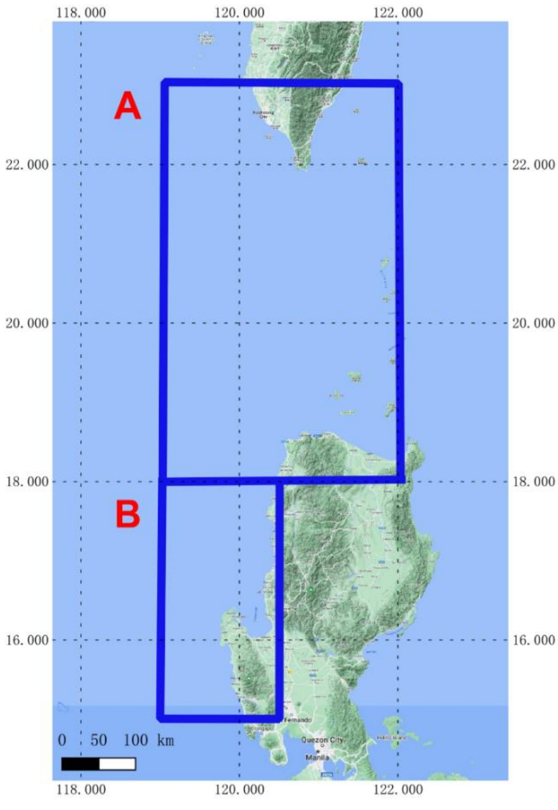

Figure 3: The two northernmost subdivisions of the Manila Trench (see Zhang, 2021, and Li, et al., 2016 for further details on the other subdivisions).

Table 1: Number of simulation runs for each earthquake magnitude interval.

M'_{Wj}	Zone A	Zone B
[7.0,7.2]	309	245
[7.2,7.4]	283	251
[7.4,7.6]	327	322
[7.6,7.8]	303	357
[7.8,8.0]	288	291
[8.0,8.2]	274	300
[8.2,8.4]	274	293
[8.4,8.6]	291	-
[8.6,8.8]	318	-
[8.8,9.0]	274	-
Total	5000	

The G-R relation, which describes the average number of earthquakes equal to or greater than a given M_W per year, is given as:

$$N(M_W) = 10^{a-bM_W} \tag{6}$$

here, *a* and *b* are the G-R curve parameters. The G-R curve parameters, based on a global seismic catalog (Li et al. 2016) for each zone, are shown in Table 2.

Table **Fout! Geen tekst met de opgegeven stijl in het document.**: G-R curve parameters in Zone A and B.

	Zone A	Zone B
A	6.20	4.96
B	1.12	0.94

The tsunami propagation simulations were conducted using the COMCOT model (Liu et al. 1998). COMCOT is based on the shallow water equations, and is implemented with linear and non-linear shallow water equations in both spherical and cartesian Coordinates. In this study, spherical coordinates were used in the propagation. As the tsunami waves approach the coastal line, the linear shallow water equations are no longer valid due to the changes in the wavelength and amplitude. The nonlinear convective inertia force and bottom friction have a significant effect on the results.

The following nonlinear shallow water equations were implemented using spherical coordinates in COMCOT;

$$\frac{\partial \eta}{\partial t} + \frac{1}{R\cos\varphi}\left\{\frac{\partial P}{\partial \psi} + \frac{\partial}{\partial \varphi}(\cos\varphi Q)\right\} = -\frac{\partial h}{\partial t} \tag{7}$$

$$\frac{\partial P}{\partial t} + \frac{1}{R\cos\varphi}\frac{\partial}{\partial \psi}\left\{\frac{P^2}{H}\right\} + \frac{1}{R}\frac{\partial}{\partial \varphi}\left\{\frac{PQ}{H}\right\} + \frac{gH}{R\cos\varphi}\frac{\partial \eta}{\partial \psi} - fQ + F_x = 0 \tag{8}$$

$$\frac{\partial Q}{\partial t} + \frac{1}{R\cos\varphi}\frac{\partial}{\partial \psi}\left\{\frac{PQ}{H}\right\} + \frac{1}{R}\frac{\partial}{\partial \varphi}\left\{\frac{Q^2}{H}\right\} + \frac{gH}{R}\frac{\partial \eta}{\partial \varphi} + fP + F_y = 0 \tag{9}$$

where η indicates the water surface elevation and *t* the time. φ, ψ represent the latitude and longitude of the Earth and R the radius of the Earth. P, Q indicate the volume fluxes in *x* (West-East) direction and *y* (South-North) directions, *h* is the water depth and g is the gravitational acceleration. *f* represents the Coriolis force coefficient and can be represented by:

$$f = \Omega \sin\varphi \tag{10}$$

Ω represents the rotation rate of the Earth. In the Cartesian Coordinates, they are implemented as:

$$\frac{\partial \eta}{\partial t} + \left\{\frac{\partial P}{\partial x} + \frac{\partial Q}{\partial y}\right\} = -\frac{\partial h}{\partial t} \tag{11}$$

$$\frac{\partial P}{\partial t} + \frac{\partial}{\partial x}\left\{\frac{P^2}{H}\right\} + \frac{\partial}{\partial y}\left\{\frac{PQ}{H}\right\} + gH\frac{\partial \eta}{\partial x} + F_x = 0 \tag{12}$$

$$\frac{\partial Q}{\partial t} + \frac{\partial}{\partial x}\left\{\frac{PQ}{H}\right\} + \frac{\partial}{\partial y}\left\{\frac{Q^2}{H}\right\} + gH\frac{\partial \eta}{\partial y} + F_y = 0 \tag{13}$$

where *(x, y)* indicates the horizontal coordinates, H indicates the total water depth, which is the sum of water surface elevation η and the water depth h. F_x and F_y represent the bottom friction in X and Y directions, respectively, and can be calculated through Manning's formula:

$$F_x = \frac{gn^2}{H^{7/3}} P(P^2 + Q^2)^{1/2} \tag{14}$$

$$F_y = \frac{gn^2}{H^{7/3}} Q(P^2 + Q^2)^{1/2} \tag{15}$$

where n represents the Manning's roughness coefficient.

The time history record of the water height at various digital gauges can be obtained as an output result for each propagation simulation. As indicated in Fig. 2, a Monte Carlo simulation that included 5000 tsunami propagation simulations were conducted. The computations were performed in parallel using six desktop computers (with different processor speeds, but which took an average of 6 hours per simulation run, representing 30,000 hours of computational time over several months).

2.4 Return period

According to Sepúlveda et al. (2019), the joint mean return period chance to exceed the tsunami height h_c can be calculated as:

$$T_R(h_c) = \frac{1}{\sum_j \sum_i \lambda^{EQ}_{M'_{Wj},x_i} P_h(h > h_c | M'_{Wj}, x_i)} \tag{16}$$

here, $P_h(h > h_c | M'_{Wj}, x_i)$ represents the chance to exceed the tsunami height h_c. This chance was calculated through the output result from the tsunami propagation simulations. The averaged recurrence rate of earthquakes of magnitude M'_{Wj} in the seismogenic region x_i can be calculated from:

$$\lambda^{EQ}_{M'_{Wj},x_i} = N\left(M_{Wj} - \frac{\Delta M_{Wj}}{2}\right) - N\left(M_{Wj} + \frac{\Delta M_{Wj}}{2}\right) \tag{17}$$

here, N represents the average earthquake recurrence, which can be obtained from the G-R model.

2.5 Sea level rise and tsunami inundation simulations

According to the Intergovernmental Panel on Climate Change 6th Assessment Report (IPCC 6AR), the global mean sea level projections for five Shared Socio-economic Pathway (SSP) scenarios for the year 2100 are shown in Table 3 (Fox-Kemper, et al., 2021).

Table 1: Global mean sea level projections for five SSP scenarios for the year 2100.

	Likely ranges [m]	Median values [m]
SSP1-1.9	0.28-0.55	0.38
SSP1-2.6	0.32-0.62	0.44
SSP2-4.5	0.44-0.76	0.56
SSP3-7.0	0.55-0.90	0.68
SSP5-8.5	0.63-1.01	0.77
SSP5-8.5 Low Confidence	0.63-1.60	0.88

Five sea level rise scenarios were considered in the tsunami inundation simulations, namely 0.0 m, 0.28 m, 0.56 m, 1.01 m, and 1.60 m, which correspond to a baseline scenario, the lower limit of the likely range of SSP1-1.9, the median value for SSP2-4.5, the upper limit of SSP5-8.5 and the upper limit of SSP5-8.5 of the low-confidence processes. Inundation maps were produced for tsunamis with return time periods of 100 years (level 1 tsunami, according to the current tsunami countermeasure philosophy in Japan, see Shibayama et al. 2013), 1,000 years (level 2 tsunami) and 10,000 years (a design level currently used by densely inhabited areas of the Netherlands). As a result, a total of 15 tsunami inundation simulations were conducted using Nays2DFlood The bathymetry was altered for each SLR inundation scenario conducted, meaning that any nonlinearity effects (see Koyano et al., 2020, 2022) are included in the results of the local propagation and inundation simulations using Nays2DFlood.

Nays2DFlood is a flood flow solver using the International River Interface Cooperative (iRIC) software developed by Professor Yasuyuki Shimizu at the University of Hokkaido. This solver treats unsteady 2-dimensional plane flows using general curvilinear coordinates and adopts the computational scheme of the Nays2DH Solver, including the CIP momentum advection method. This solver is able to conduct tsunami inundation simulations. Previous research using Nays2DFlood is described, for instance, by Hao et al. (2021) and Ali et al. (2017).

The elevation data used for the baseline scenario (representing present date conditions) is shown in Fig. 4. The elevation data was obtained from USGS elevation tiles (SRTM) with a resolution of 70 m, which was fed into Nays2DFlood. The initial water surface condition for the rivers was set as a constant slope of 0.0001 along the main channels, to give an almost horizontal level that was not that different to the sea water level. According to Collection of Hydraulic Formulae (Japan Society of Civil Engineers, 1999), different Manning's roughness coefficients were set, depending on the type of land use area, as shown in Table 4 and Fig. 5. The total simulation time was set to 60 minutes and the time step as 0.5 seconds.

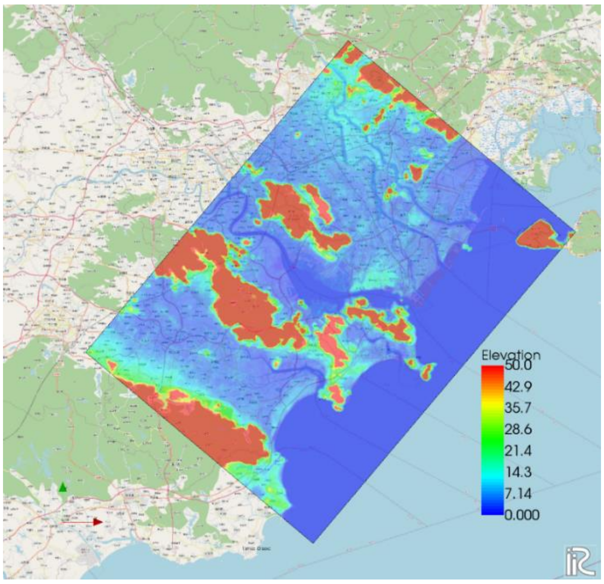

Figure 4: Elevation data for Shantou. Data obtained from USGS. Unit: m.

Table 4: Manning's roughness coefficient according to area.

Descriptions	Manning's roughness coefficient
Sea	0.025
River	0.025
High building density area	0.08
Low building density area	0.04
Forested mountain	0.03

2.6 Inundation safety thresholds

To estimate the level of threat posed by tsunami inundation, not only the water depth but also the speed of the water flow should be taken into consideration. According to Takagi et al. (2016), during typhoon Haiyan, when the flow speeds and heights were relatively small, such as 0.6 m/s and 0.6 m respectively, people successfully evacuated from a hotel in Tacloban city. On the other hand, Wright et al. (2010) indicated that the upper safe limit of the product depth x velocity *(dv)* for adult pedestrians is 1.2 m^2/s. This upper limit of 1.2 m^2/s was adopted in the research of Nagai et al. 2020, and also in the present study as the threshold after which any inundation will result in casualties.

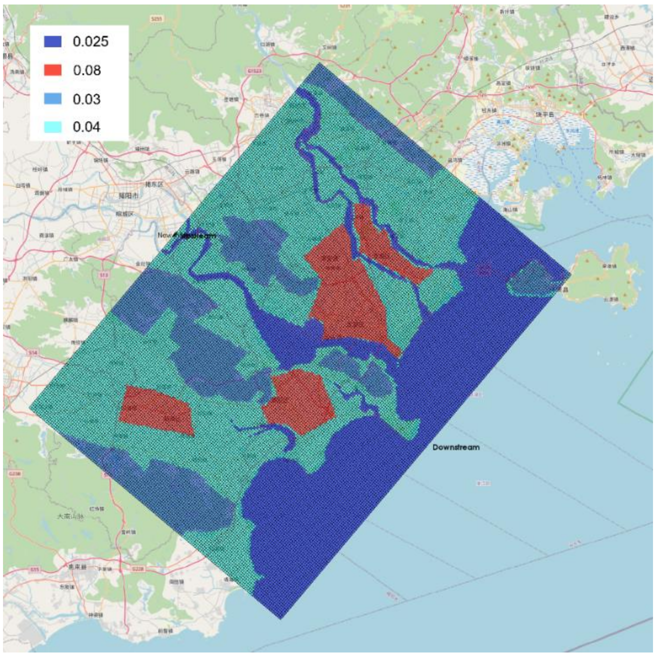

Figure 5: Distribution of Manning's roughness coefficient according to land use type.

3 Results

3.1 Hazard curve

After 5,000 tsunami propagation simulations were conducted using COMCOT, the Peak Nearshore Tsunami Amplitude (PNTA) curve could be obtained for the various return periods, as shown in Fig. 6. The PNTA for a return time period under 1,000 years is relatively low, which indicates that the current tsunami risk at Shantou is modest, particularly considering the threat the Manila Trench poses to other areas around it (Wu and Huang, 2009). However, this is expected to increase in the future due to ongoing SLR, as will be explained later.

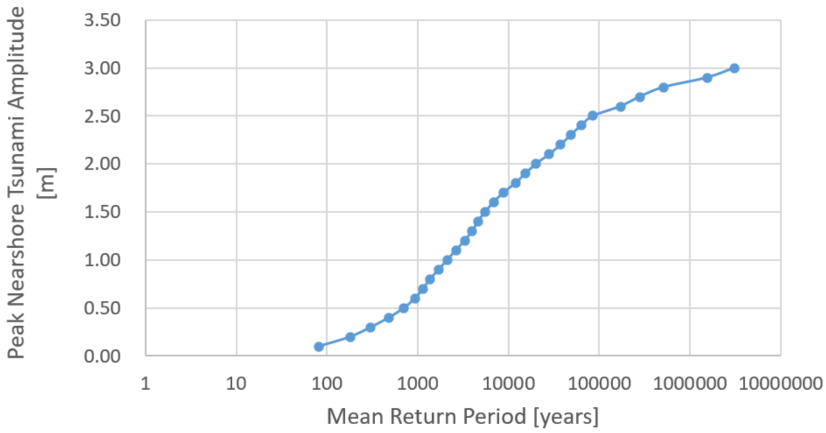

Figure 6: Expected offshore tsunami hazard curve at Shantou.

3.2 Tsunami inundation simulations

Three representative tsunami waveforms corresponding to the PNTA values shown in Fig. 6 were picked up among the 5000 tsunami propagation simulations, which formed the starting point of the inundation simulations. The fault parameters and the PNTA corresponding to the different mean return periods are summarized in Table 5.

Table 5: Sample tsunami waveforms for the inundation simulations for different return periods.

Parameter	Return period [year]		
	100	1,000	10,000
M_w	7.69	8.26	8.77
$E_{pi\ x}$	119.30	119.10	119.64
$E_{pi\ y}$	22.25	22.78	22.52
Depth [km]	44.75	31.72	33.82
Length [km]	109.88	224.19	429.95
Width [km]	56.85	84.97	122.65
Dislocation [m]	2.30	5.27	11.23
Strike angle [°]	33	33	33
Dip angle [°]	17.9	17.9	17.9
Rake angle [°]	90	90	90
PNTA [m]	0.16	0.68	1.77

The shapes of the tsunami waveforms summarized in Table 5 are shown in Fig. 7 (t=0 is the time of the earthquake, so it takes roughly two and a half hours for the tsunami to propagate from the north of the Manila Trench to the south coastline of China). Note that only the first hour of the tsunami wave was used in the inundation simulations (as the subsequent part of the waveform was deemed unlikely to worsen the inundation).

The inundation process can be seen in Fig. 8, which describes the water surface elevation at Shantou during the tsunami inundation in the case of a tsunami height with a return period of once in 10,000 years with no sea level rise.

Following the inundation simulations performed using Nays2DFlood, the distribution of *dv* product for the three return periods and 5 SLR scenarios was mapped across the study area, as shown in Figs. 9 to 11 (each inundation simulation was conducted by incorporating the SLR into the bathymetry of the area, in order to capture any nonlinear effects, see Koyano et al., 2020, 2022). Red color indicates the areas where $dv \geq 1.2$ m^2/s.

It can be seen from Figures 9 to 11 that, and with reference to Fig. 1, since Rongjiang River flows through Shantou city and empties into the South China Sea at Shantou Harbor, the area near the river would likely suffer the worst inundation, even for low tsunami heights and the modest SLR scenarios. Due to the low elevation and flat terrain in Chaonan District, this area can also suffer from tsunami inundation, especially for SLR scenarios over 0.56 m. One of the main reasons for the potential inundation in the Chaonan District is Lianjiang River, which flows through Chaonan District and empties into the South China Sea at Haimen Harbor. Besides, the area to the east of Jieyang city also appears to be in danger for SLR scenarios of 1.01 m and above, as the tsunami can propagate through Fengjiang River, which is connected to Rongjiang River.

The relation between the mean SLR scenarios and the expected flooded area where the values of $dv \geq 1.2$ m^2/s for different return periods is shown in Fig. 12.

From Fig. 12, it is clear that in the future, as the mean sea level rises, so will the expected flooded area increase, unless significant adaptation countermeasures are implemented. However, the expected tsunami return time period has a comparatively small influence in the increase in expected flooded areas, especially for the more onerous SLR scenarios (mean sea level rises 1.01 m and 1.60 m). One of the reasons is that the expected tsunami height in Shantou city is relatively low, even for the case of a 10,000-year return period.

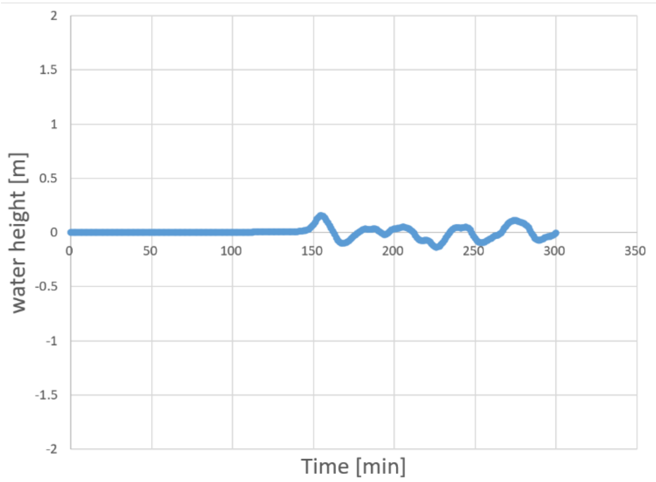

(a)

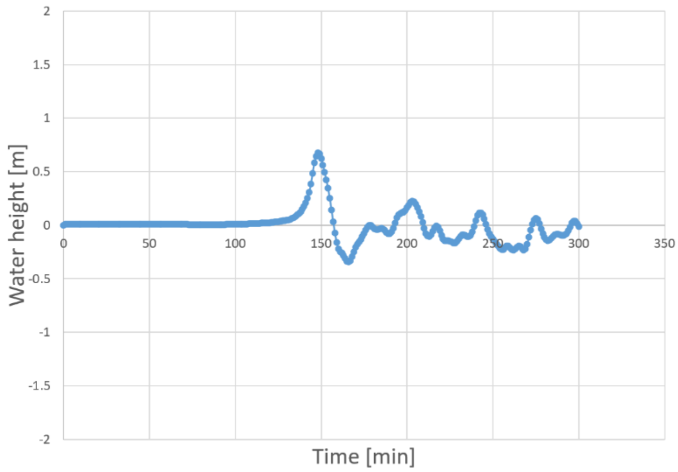

(b)

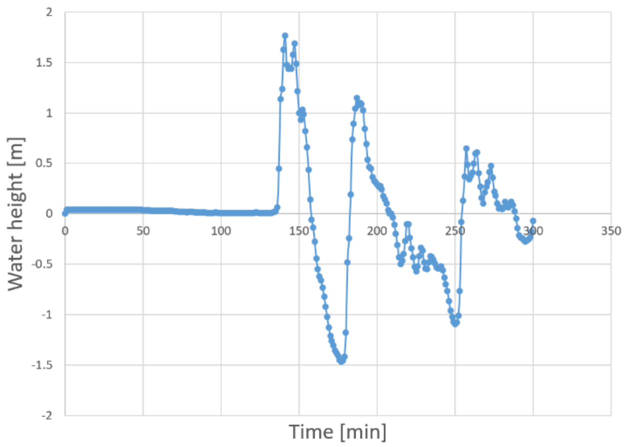

(c)

Figure 7: Representative tsunami waveforms for different mean return periods. (a) 100 years, (b) 1,000 years, (c) 10,000 years.

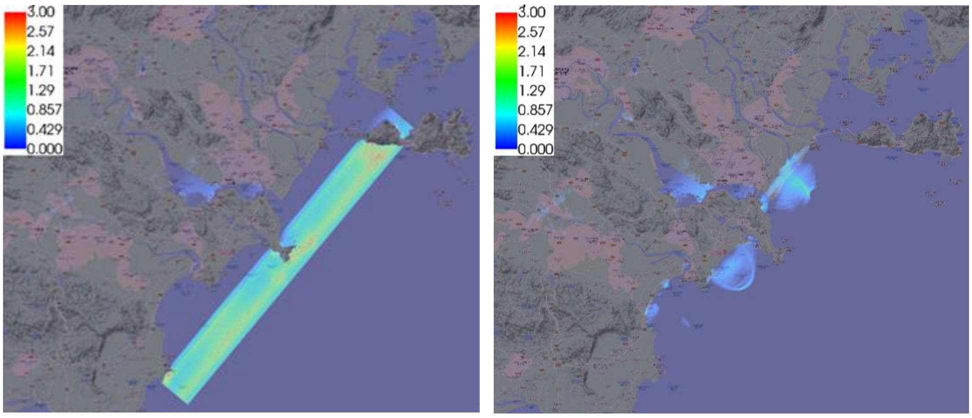

(a) (b)

Figure 8: Water surface elevation of a tsunami height with a return period of 10,000 years with 0.0 m sea level rise. (a) 20 min, (b) 40 min. Unit: m.

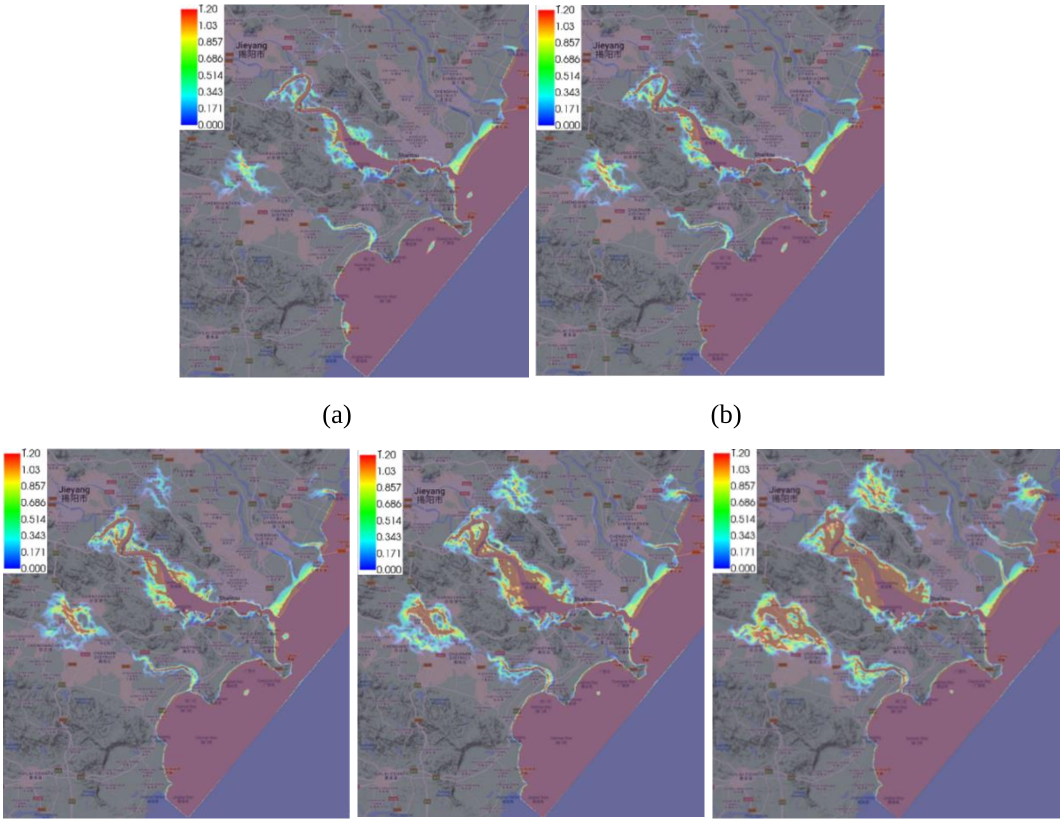

(a) (b)

(c) (d) (e)

Figure 9: Distribution of *dv* product for tsunami heights with a return period of 100 years. (a) 0 m sea level rise, (b) 0.28 m sea level rise, (c) 0.56 m sea level rise, (d) 1.01 m sea level rise, (e) 1.60 m sea level rise. Unit: m.

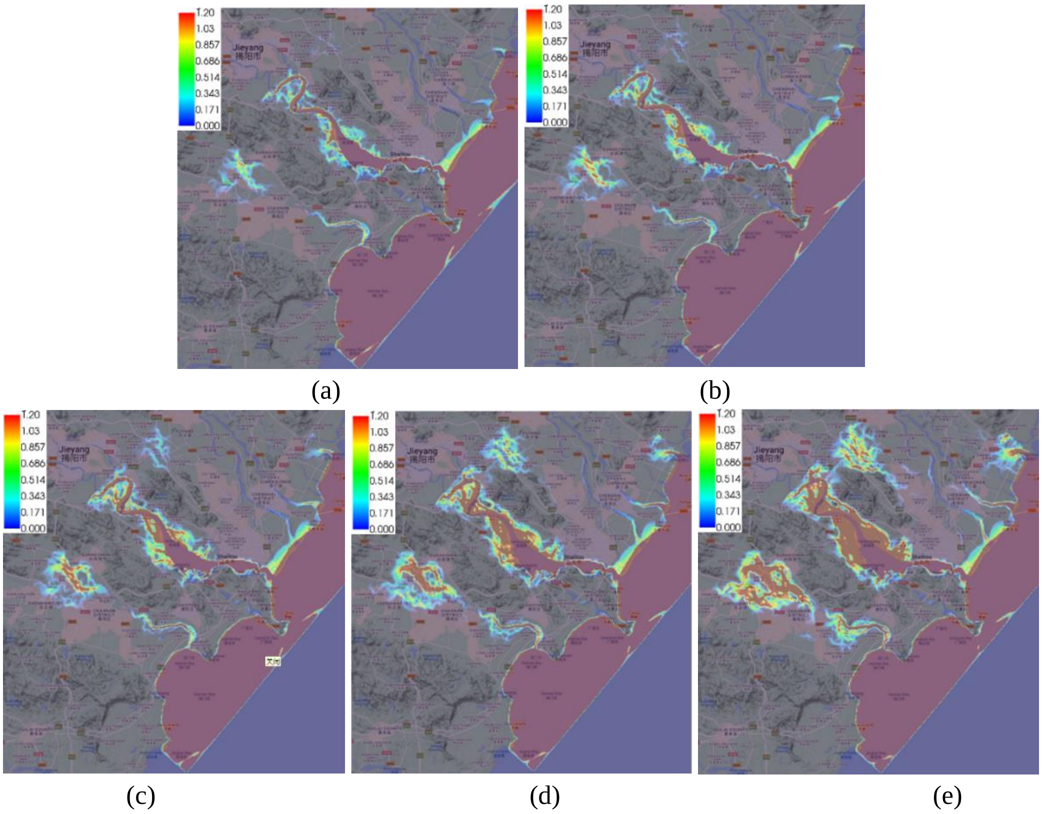

Figure 10: Distribution of *dv* product for tsunami heights with a return period of 1,000 years. (a) 0 m sea level rise, (b) 0.28 m sea level rise, (c) 0.56 m sea level rise, (d) 1.01 m sea level rise, (e) 1.60 m sea level rise. Unit: m.

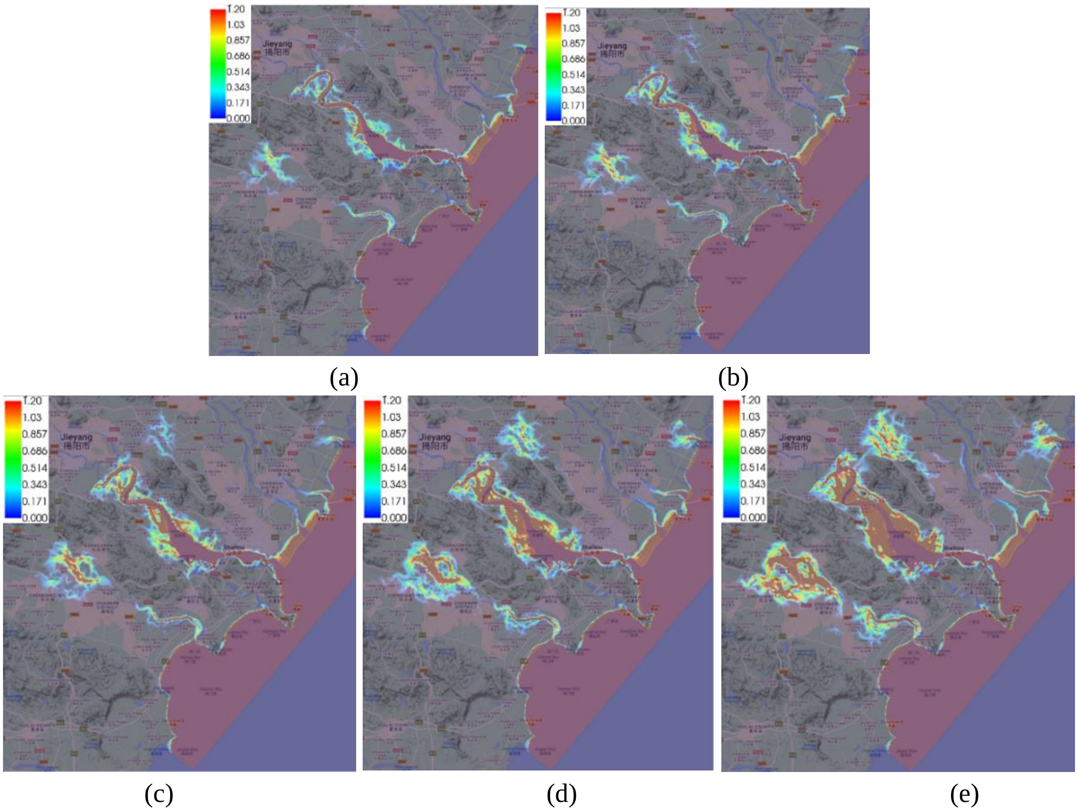

Figure 11: Distribution of *dv* product for tsunami heights with a return period of 10,000 years. (a) 0 m sea level rise, (b) 0.28 m sea level rise, (c) 0.56 m sea level rise, (d) 1.01 m sea level rise, (e) 1.60 m sea level rise. Unit: m.

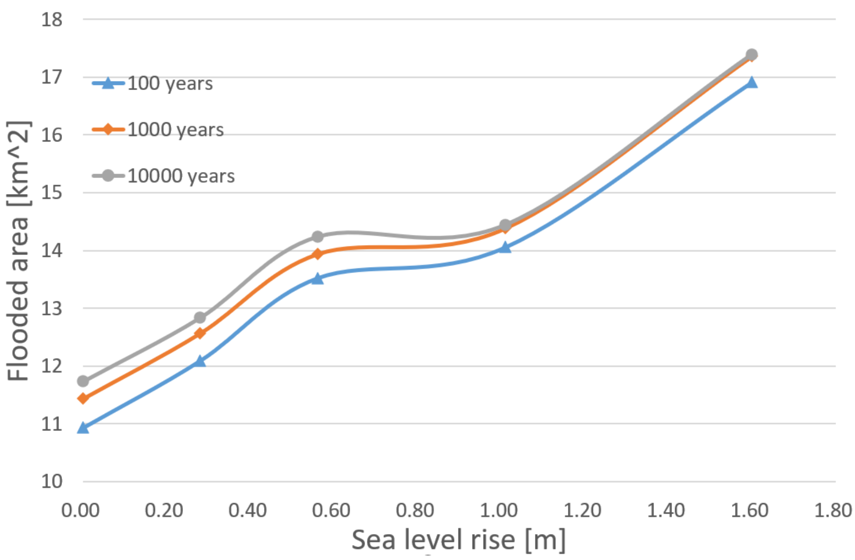

Figure 12: Relation between mean SLR scenarios and expected flooded area for different tsunami return periods.

4 Discussion

4.1 Comparisons with previous research

This paper made use of a Monte Carlo-type probabilistic tsunami hazard assessment (PTHA) that employed a stochastic earthquake generation model (similar to the work detailed in Li et al. 2016). In the research of Li et al. (2016), a wide range of earthquake magnitudes, ranging from 7.0 to 9.0, were considered along the Manila Trench from around 12.5°N to 23°N, using both uniform and heterogeneous slips. In total, nearly 30,000 earthquakes were simulated by Li et al. (2016), considering both a seismic and geodetic catalog. However, the present study considered only Shantou as a case study, and thus focused only on 5,000 earthquakes that could be generated between 15°N and 23°N along the Manila Trench, using a seismic catalog with a uniform slip model. Due to the differences in the simulation conditions, the obtained hazard curves are thus slightly different to those in Li et al. (2016), where the PNTA indicates tsunami waveforms of 0.1 m and 1 m for return periods of 100 and 1,000 years, respectively (compared to 0.15 and 0.65 m for present research).

4.2 Limitations

As mentioned earlier, the PTHA method used in the present research only employed a seismic catalog with a uniform slip model. According to Li et al. (2016), a geodesy-based catalog results in tsunami waves 2-4 times higher than those using a seismic catalog, for the same return period, especially for return periods shorter than 1000 years. On the other hand, a non-uniform slip distribution results in wave amplitudes 20-60% larger than for the uniform slip model for a 500 years return period, and the effect of non-uniform slip distribution is more significant for longer return periods (Li et al. 2016). It is obvious that to obtain a more accurate PTHA result, both geodesy-based and seismic catalog should be taken into consideration when the return period is short, while a non-uniform slip distribution should be employed when the return period is longer. Nevertheless, the present methodology served to highlight how a full tsunami inundation hazard assessment should be carried out, including both tsunami propagation and inundation simulations. Such results can provide a better assessment of the likely risks than only assessing the waveforms at the coastline.

Regarding the tsunami propagation simulations, the movement of the fault was modeled in COMCOT to calculate the deformation of the seafloor, and this could be different if the fault ruptures in a different pattern than that which was modeled (for example, if the rupture speed were to be different). Generally, a lower rupture speed, i.e., 500 m/s or 1000 m/s, would lead to a lower maximum water surface elevation compared with a high rupture speed, i.e., 1500 m/s or 2000 m/s. The direction of the rupture of the fault would also change for different rupture speeds (Xintong et al. 2019).

For the tsunami inundation simulations, it can be noticed from Fig. 4 that the SRTM data obtained from USGS may not accurately represent the terrain of the case study area. The elevation of the riversides (including the presence of any river levees) might not be accurate, which can severely limit the accuracy of inundation simulations (and which highlights the need to obtain more accurate data, although this can be challenging for the study area). Furthermore, the initial conditions of water depth at the upstream reaches of the rivers in Shantou can be modelled more accurately. The effect of water flow along the rivers, especially Rongjiang River, the widest river in Shantou, was not included when conducting tsunami inundation simulations.

Finally, another limitation of the present study resides in the use of global SLR projections, rather than regional level ones. Li et al (2024) analyzed tidal gauge data along the South China Sea coast, and found that SLR was an average of 4.0 mm / year, similar to the global SLR rate, although the study did not include the city of Shantou. Other analysis by Li et al (2024), using tidal and satellite observations also shows rates of regional SLR to be 3.4 mm per year in the period 1980-2021, although again this does not include the city of Shantou. Given that the regional rate of SLR thus appears to be similar to that at the global level, but that no local SLR measurements are available for Shantou, the authors chose to use the global level, although this represents a limitation of this study (as it may be that projections for Shantou might be slightly different).

4.3 Implications of future SLR on tsunami hazard

From the tsunami inundation simulations (see Figs. 9 to 11), it would appear that the area to the northwest of Chaonan District can be affected by tsunami waves, and that this hazard could increase in the future due to SLR. The same is true for the area next to the Rongjiang River. A tsunami early warning system and adaptation countermeasures that could prevent tsunamis from propagating along Lianjiang River, which connects Chaonan District and the South China Sea, should thus be implemented, which could for example include constructing storm surge/tsunami barriers at the entrance of key sections of the river. Regarding the area nearby Rongjiang River, instead of constructing dams across the river, placing wave-dissipation armor or planting trees might be useful, given that there are many harbors that exist along this waterway and that these extend until Jieyang city. The area to the east side of Jieyang city can be expected to suffer less inundation than the two areas just mentioned, given that the origin of this flooding would be tsunami propagation upstream of the Rongjiang River, through a small river (Fengjiang River, and where a small gate could be constructed to prevent propagation along the river to the east of Jieyang city).

Tsunami awareness is key to prevent the loss of life. According to Suppasri et al. (2013), during the 2011 Tohoku Tsunami in the east of Japan, people who had high tsunami awareness spent less time on evacuating than those with low awareness, which highlights the importance of tsunami awareness education. However, in the case of Shantou, a tsunami from the Manila Trench would arrive two hours after the earthquake happens, which gives ample time for citizens to evacuate (compared to the case of other tsunamis such as the 2011 Tohoku Earthquake and Tsunami, Mikami et al., 2012, or the 2018 Palu Tsunami, Takagi et al., 2019). Nevertheless, a tsunami originating from the Baiyun Slide region (Ren et al., 2023) would arrive much quicker. In that sense the citizens of Shantou should be educated about what to do in such events, and about the locations of shelters and the evacuation routes.

4.4 Future research

In order to obtain a more accurate assessment of the tsunami hazard in Shantou, both tsunami propagation and inundation models need to be continuously improved in the future, including using more accurate bathymetric and topography data. Both geodesy-based and seismic catalogs can be employed in PTHA, and nonuniform slip distribution should also be considered.

Regarding inundation simulations, as mentioned above, the correct estimation of flow patterns is of crucial importance, especially given that under present day conditions the expected tsunami heights in Shantou are rather modest. However, future SLR will increase the risk (as also highlighted by Koyano et al., 2022 and Nagai et al., 2019) although uncertainties regarding the rate at which the water is rising (related to both gaps in knowledge about how the planet works and uncertainties regarding future greenhouse gas emission patterns) makes it challenging to estimate future return periods.

5 Conclusions

This study showcased a methodology of how to conduct a Monte-Carlo type of Probabilistic Tsunami Hazard Assessment (PTHA) of waveforms originating from Manila Trench and propagating to Shantou city in southeast of China using the COMCOT model. The result of the simulations indicates that the Peak Nearshore Tsunami Amplitude (PNTA) for return time periods of 100, 1,000, 10,000 years is 0.15 m, 0.65 m, 1.75 m, respectively. Five different sea level rise scenarios were also simulated, namely 0 m, 0.28 m, 0.56 m, 1.01 m, and 1.60 m, with maps of the expected inundation extent plotted, focusing on areas were the product of the water depth d [m] and velocity v [m/s] is greater than 1.2 m^2/s. The inundation simulation results indicate that, as sea level rise rises, the expected flooded area where the product of dv is greater than 1.2 m^2/s also increases.

To adapt to sea level rise and reduce overall tsunami risks, gates could be constructed across Lianjiang River and Fengjiang River, which would prevent a wave travelling upstream towards the Chaonan District and the east of Jieyang city, respectively. Along Rongjiang River, the widest river in Shantou, planting trees and setting wave-elimination blocks are recommended to avoid damage to harbors. Improving tsunami awareness and education for citizens on how to evacuate is also warranted.

Monte-Carlo type PTHA can help to quantify the hazard of tsunamis to a given area, allowing for a range of earthquake source regions and parameters to be scrutinized. It is obvious that such hazard assessment approach should be prioritized in coastal risk management policy. However, further research is still needed to implement both geodesy-based and seismicity-based catalogs, and the use of non-uniform slip distributions in PTHA. Besides, such endeavors would doubtlessly benefit from more accurate bathymetric and topography data, not only in Shantou but also in many other coastal areas.

Acknowledgements

A part of the present work was performed as a part of activities of Research Institute of Sustainable Future Society, Waseda Research Institute for Science and Engineering, Waseda University. The present work was financially supported by the Japan Society for the Promotion of Science (JSPS) KAKENHI Grant Number 20KK0107.

Author contributions (CRediT)

TZ[1]: Conceptualization, Data curation, Formal Analysis, Methodology, Resources, Software, Validation, Visualization, Writing – original draft, Writing – review & editing. ME[2]: Conceptualization, Methodology, Resources, Software, Validation, Writing – original draft, Writing – review & editing, Supervision. TM[3]: Methodology, Resources, Software, Writing – review & editing, Supervision. TS[4]: Writing – review & editing, Supervision.

Data access statement

The data acquired in the study and reported in this paper is available from the authors upon reasonable request.

Author contributions (CRediT)

All authors declare that they have no conflict of interest.

References

Ali, M.A., Kimura, I., Abdelrazek, A.M., Shimizu, Y.(2017) Large scale flood modelling using hyper grid approach. *Journal of Japan Society of Civil Engineers, Ser. B1, Hydraulic Engineering,* Vol. 73, No. 4, I_319-I_324, 2017.

Esteban, M., Takabatake, T., Nagai, R., Koyano, K. and Shibayama, T. (2024) Sea level rise and tsunami risk, in Goda, K., Risi, R., Gusman, A. R. and Nistor, I. (eds) *Probabilistic Tsunami Hazard and Risk Analysis - Towards Disaster Risk Reduction and Resilience.* Elsevier.

Fox-Kemper, B., H.T. Hewitt, C. Xiao, G. Aðalgeirsdóttir, S.S. Drijfhout, T.L. Edwards, N.R. Golledge, M. Hemer, R.E. Kopp, G. Krinner, A. Mix, D. Notz, S. Nowicki, I.S. Nurhati, L. Ruiz, J.-B. Sallée, A.B.A. Slangen, and Y. Yu,

(2021) Ocean, Cryosphere and Sea Level Change. In *Climate Change 2021: The Physical Science Basis. Contribution of Working Group I to the Sixth Assessment Report of the Intergovernmental Panel on Climate Change* [Masson-Delmotte, V., P. Zhai, A. Pirani, S.L. Connors, C. Péan, S. Berger, N. Caud, Y. Chen, L. Goldfarb, M.I. Gomis, M. Huang, K. Leitzell, E. Lonnoy, J.B.R. Matthews, T.K. Maycock, T. Waterfield, O. Yelekçi, R. Yu, and B. Zhou (eds.)]. Cambridge University Press, Cambridge, United Kingdom and New York, NY, USA, pp. 1211–1362, doi: 10.1017/9781009157896.011.

GEBCO Compilation Group (2021) GEBCO 2021 Grid (doi:10.5285/c6612cbe-50b3-0cff- e053-6c86abc09f8f)

Gu, G., Zhou, W., and Wang, R., (eds.) (1989): Catalogue of Chinese Earthquakes (1831 B.C. - 1969 A.D.). Science Press, Beijing, China; English translation by Li Zengquan et al. provided through UNESCO, 872 pages.

Hao, C., Yunus, A. P., Subramanian, S. S., and Avtar, R. (2021) Basin-wide flood depth and exposure mapping from SAR images and machine learning models, Journal of Environmental Management, Volume 297, 113367, ISSN 0301-4797.

Hirschfeld, D, Boyle, R., Nicholls, R. J., Behar, D., Esteban, M., Hinkel, J., Smith, G. and Hanslow, D. J. (2024) Practitioners needs to adapt to sea-level rise: distilling information from global workshops, *Climate Services*, 34, 100452.

Japan Society of Civil Engineers, (1999) *Collection of Hydraulic Formulae*, p. 89.

Hou, J., Yu, F., Wang, P. (2014) Numerical study on tsunami inundation for the urban area of Shantou City, *Marine Forecasts*, 31(4).

Jean R., Bernard P., Jérôme A., Update of the tsunami catalogue of New Caledonia using a decision table based on seismic data and marigraphic records, *Nat. Hazards Earth Syst. Sci*., 19, 1471–1483, 2019.

Kanamori, H. (1977) The energy release in great earthquakes. *J Geophys Res* 82:2981-2987.

Kirby, S., Geist, E., Lee, W.H.K., Scholl, D., Blakely, R., 2006. Tsunami source characterization for Western Pacific subduction zones: a preliminary report. In: USGS Tsunami Sources Workshop 2006. Houston, TX.

Koyano, K., Takabatake, T., Esteban, M. and Shibayama, T. (2022) Magnification of tsunami risks due to sea level rise along the eastern coastline of Japan, *Journal of Coastal and Hydraulic Structures*, https://doi.org/10.48438/jchs.2022.0012

Koyano, K., Takabatake, T., Esteban, M. and Shibayama, T. (2020) Influence of edge waves on tsunami characteristics along Kujukuri beach, Japan, Journal of Waterway, Port, Coastal and Ocean Engineering 147 (1) doi.org/10.1061/(ASCE)WW.1943-5460.0000617

Li, L., Switzer, A.D., Chan, C.-H., Wang, Y., Weiss, R., Qiu, Q. (2016) How heterogeneous coseismic slip affects regional probabilistic tsunami hazard assessment: a case study in the South China Sea. J. Geophys. Res.: Solid Earth 121 (8), 6250–6272.

Li, Y., Mu, L., Dawei, Y., Wang, J., Niu, Q. and Liao, X. (2024) Changes in sea level along the South China Sea coast based on the homogenized tide gauge data. *Journal of Marine Science Engineering Eng.* 2024, *12*(3),

Li, W., Wang, H. Xiang, W, Wang, A., Xu, W., Jiang, Y., Wu, X., and Quan, M. (2024) Sea-level change in coastal areas of China: Status in 2021, *Advances in Climate Change Research*, 15 (3) 515-524

Liu, P.L.-F., Woo, S.-B. and Cho, Y.-S. (1998). Computer Programs for Tsunami Propagation and Inundation. Cornell University.

Mikami, T., Shibayama, T., Esteban, M. and Matsumaru, R., (2012) Field Survey of the 2011 Tohoku Earthquake and Tsunami in Miyagi and Fukushima Prefectures, *Coastal Engineering Journal (CEJ)*, Vol. 54, No. 1, pp. 1-26

Nagai, R., Takabatake, T., Esteban, M, Ishii, H., Shibayama, T., (2020) Tsunami risk hazard in Tokyo Bay: The challenge of future sea level rise, *International Journal of Disaster Risk Reduction* 45 101321.

NOAA, DOI:10.7289/V5PN93H7, accessed on 2023/7/20.

Papazachos, B. C., E. M. Scordilis, D. G. Panagiotopoulos, C. B. Papazachos, and G. F. Karakaisis (2004), Global relations between seismic fault parameters and moment magnitude of earthquakes, *Bull. Seismol. Soc*. Greece, XXXVI, 1482–1489.

Peter B., Domenico G. (2010) The moment magnitude and the energy magnitude: common roots and differences. Journal of Seismology, Springer Verlag, 15 (2), pp.411-427. 10.1007/s10950-010-9219-2. hal-00646919

Ren, Z., Liu, H., Li, L. *et al.* On the effects of rheological behavior on landslide motion and tsunami hazard for the Baiyun Slide in the South China Sea. *Landslides* 20, 1599–1616 (2023). https://doi.org/10.1007/s10346-023-02058-y

Sepúlveda, I., Liu, P. L.-F., & Grigoriu, M. D. (2019). Probabilistic tsunami hazard assessment in South China Sea with consideration of uncertain earthquake characteristics. *Journal Geophysical Researcher: Solid Earth*, *124*, 658–688.

Shibayama, T., Esteban, M., Nistor, I., Takagi, H., Danh Thao, N., Matsumaru, R., Mikami, T., Aranguiz, R., Jayaratne, R. and Ohira, K. (2013) Classification of Tsunami and Evacuation Areas, *Natural Hazards*, 67 (2), 365-386.

Shibayama, T. and Esteban, M. (2023) *Coastal Disaster Surveys and Assessment for Risk Mitigation*, Edited Book, CRC Press (Taylor & Francis Group), Boca Raton.

Suppasri, A., Shuto, N., Imamura, F. et al. (2013) Lessons Learned from the 2011 Great East Japan Tsunami: Performance of Tsunami Countermeasures, Coastal Buildings, and Tsunami Evacuation in Japan. *Pure Appl. Geophys*. 170, 993–1018 https://doi-org.waseda.idm.oclc.org/10.1007/s00024-012-0511-7.

Takabatake, T., Han, D. C., Valdez, J. J., Inagaki, N., Mall, M., Esteban, M. and Shibayama, T. (2022) Three-dimensional physical modelling of tsunamis generated by partially submerged landslides, *Journal of Geophysics Research –Oceans*, 127 (1) https://doi.org/10.1029/2021JC017826

Takabatake, T., Mall, M., Han, D. C., Inagaki, N., Kisizaki, D., Esteban, M. and Shibayama, T. (2020) Physical modelling of tsunamis generated by subaerial, partially submerged and submarine landslides, *Coastal Engineering Journal* (CEJ), 62 (4) 582-601, https://doi.org/10.1080/21664250.2020.1824329

Takagi, H.,Li, S., de Leon, M., Esteban, M., Mikami, T., Matsumaru, R., Shibayama, T. ad Nakamura, R. (2016) Storm surge and evacuation in urban areas during the peak of a storm, *Coastal Engineering*, 108 1–9, https://doi.org/10.1016/j.coastaleng.2015.11.002

Takagi, H., Pratama, M. B., Shota, K., Esteban, M., Aranguiz, R., and Ke, B. (2019) Analysis of generation and arrival time of landslide tsunami to Palu City due to the 2018 Sulawesi Earthquake, *Landslides* 16, 983-991.

Wu, T.R., Huang, H. C. (2009) Modeling tsunami hazards from Manila trench to Taiwan, *Journal of Asian Earth Sciences* 36 21-28.

Wright, K., Doody, B.J., Becker, J. McClure, J., (2010) Pedestrian and Motorist Flood Safety Study: A Review of Behaviours in and Around Floodwater and Strategies to Enhance Appropriate Behaviour, *GNS Science*,. Report 2010/51 (91 pp.).

Xintong, X., Chuanxu, C., Linlin, L., Shiguo, W., David A. Yuen, Dawei, W., (2019) Tsunami hazard assessment for atoll islands inside the South China Sea: A case study of the Xisha Archipelago, *Physics of the Earth and Planetary Interiors* 290 20–35.

Yi Xiaolei, Yu Fujiang, W.T. Wong, Yu Fujiang (2007) National Report of China, IOC/PTWS-XXII/14.4, Guayaquil, Ecuador, p. 6-8.

Yingchun, L., Angela, S., Shuo M. Wang, Yaolin, S., Hailing, L., David A. Yuen, (2007) Tsunami hazards along Chinese coast from potential earthquakes in South China Sea, *Physics of the Earth and Planetary Interiors* 163 233-244.

Zhang, T. (2021). Modeling Tsunami Hazards from Manila Trench to the Southeast Coastline of China, Graduation Thesis, Waseda University.